Single-Spin Readout in a Double Quantum Dot Including a Micromagnet

Yun-Sok Shin,[1,*] Toshiaki Obata,[1] Yasuhiro Tokura,[1,2] Michel Pioro-Ladrière,[1] Roland Brunner,[1] Toshihiro Kubo,[1] Katsuharu Yoshida,[1] and Seigo Tarucha[1,3,4]

[1]*Quantum Spin Information Project, ICORP, JST, Atsugi-shi, Kanagawa 243-0198, Japan*
[2]*NTT Basic Research Laboratories, NTT Corporation, Atsugi-shi, Kanagawa 243-0198, Japan*
[3]*Institute for Nano Quantum Information Electronics, The University of Tokyo, Komaba, Meguro-ku, Tokyo, Japan*
[4]*QPEC and Department of Applied Physics, University of Tokyo, Hongo, Bunkyo-ku, Tokyo 113-8656, Japan*

(Received 27 October 2009; published 28 January 2010)

We use photon-assisted tunneling (PAT) and an inhomogeneous Zeeman field to demonstrate spin-selective PAT readout with a double quantum dot. The inhomogeneous Zeeman field is generated by a proximal micromagnet, which provides different stray fields between the two dots, resulting in an energy difference between the interdot PAT of the up-spin state and that of the down-spin state. We apply various external magnetic fields to modify the relative filling weight between the up-spin and down-spin states and detect it by using a charge detection technique to probe the PAT induced charge delocalization in the double dot.

DOI: 10.1103/PhysRevLett.104.046802 PACS numbers: 73.23.−b, 03.67.Lx, 73.63.Kv

The readout of single electron spins in semiconductor quantum dots (QDs) is crucial for implementing spin-based quantum computing with QDs [1]. A quantum bit (qubit), the fundamental unit of a quantum computer, can be prepared by superposing the two Zeeman spin states for an individual electron. Various techniques have recently been developed to manipulate and readout electron spins in semiconductor QDs [2–6]. Spin readout in single QDs [7–10] has been demonstrated by using a technique that combines charge sensing and spin-to-charge conversion. To date most of the readout experiments have been performed for only one of the two spin orientations and in a destructive manner.

For double QDs (DQDs) [11–13] the readout of the electron spin has only been theoretically suggested. Barret and Stace [12] proposed a nondestructive continuous spin readout scheme that employed photon-assisted tunneling (PAT) and inhomogeneous Zeeman energies between the two dots. PAT allows interdot electron tunneling by conserving the energy and the angular momentum of the spin [14] when the photon energy is equivalent to the energy difference between Zeeman substates with the same spin configuration. In this case an electron becomes delocalized between the two dots and gives rise to a change in the static DQD charge state before the spin can relax to the ground state. Therefore, the PAT induced charge delocalization can be detected before the spin state relaxes [7]. For inhomogeneous Zeeman energies between the two dots, the PAT conditions for the up spin and down spin are different, thus enabling the readout of different spin configurations. To realize a relevant difference between the Zeeman energies of the two dots, we can use the stray field of a micromagnet [5], an inhomogeneous nuclear field [6], or materials with different g factors for the two dots [15].

In this Letter we present the experimental realization of a continuous PAT spin readout scheme [12] in a lateral DQD achieved by using a micromagnet technique. Figure 1(b) shows a scanning electron microscope (SEM) image of the device. A two-dimensional electron gas (2DEG) with the density of 2.0×10^{11} cm^{-2} lies 100 nm below the surface of the n-AlGaAs/GaAs substrate and is

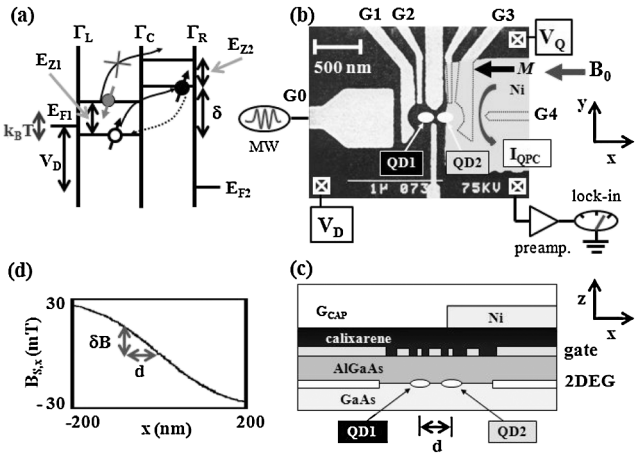

FIG. 1. (a) Schematic energy diagram for PAT spin readout with the Zeeman energies (E_{Z1} and E_{Z2}) for each dot, the energy separation δ, and the voltage bias V_D across the DQD. (b) SEM image of a lateral DQD including a Ni micromagnet, where M and ⟵ denote the magnetization of the magnet and the direction parallel to B_0, respectively. Two white circles, labeled QD1 and QD2, denote the QDs. $V_{Q(D)}$ and I_{QPC} are the voltage bias across the QPC (DQD) and the QPC current, respectively. The gates are labeled G0 to G4 clockwise and ⊠ indicates the Ohmic contacts. (c) Cross section of the device across two QDs. The two QDs are defined in the 2DEG formed at the n-AlGaAs/GaAs interface by Schottky gates. The calixarene layer isolates both the Ni magnet and the G_{CAP} from the Schottky gates. (d) Stray field $B_{S,x}$ of the magnet as a function of x, where QD2 is located at $x = 0$. d and δB correspond to the interdot spacing and the difference between the Zeeman fields of the two dots, respectively.

depleted by negatively biasing the Schottky gates labeled G0, G1, . . ., and G4. Two QDs and a quantum point contact (QPC) are defined in the 2DEG. Gates G1 and G3 are used to map the stability diagram for a DQD denoted by QD1 and QD2. Continuous microwaves (MW) applied to gate G0 provide an oscillating electric field to generate photons. A 1-μm-wide, 0.3-μm-thick, and 20-μm-long Ni magnet is placed on top of the DQD, which is separated from the metal gates by a 100-nm-thick calixarene insulation layer. The entire SEM image window is covered with a 400-nm-thick gate G_{CAP} to protect the micromagnet from oxidization and to reduce background charge noise [16]. The micromagnet provides a stray magnetic field parallel ($B_{S,x}$) and perpendicular ($B_{S,y}$, $B_{S,z}$) to its magnetization M in the x direction. The gradient of the parallel field, $\Delta B_{S,x}/\Delta x$, in the 2DEG plane is 0.17 T/μm near the edge ($x = 0$ nm) of the magnet and gradually decreases to zero within a distance of 0.3 μm as shown in Fig. 1(d). This provides a Zeeman field difference δB of about 17 mT between QD1 at $x = -100$ nm and QD2 at $x = 0$ nm. The left edge of the magnet and QD2 are almost aligned; thus, only QD1 experiences the stray Zeeman field $B_{S,x}$. The gradient of the perpendicular stray field, $\Delta B_{S,z}/\Delta x$, is about 0.07 T/μm, which might cause spin rotation in the presence of electron spin resonance [5,17,18]. Since we are not working under this condition, $\Delta B_{S,z}$ can be neglected. The gradient of the perpendicular stray field $\Delta B_{S,y}/\Delta x$ is of the order of 10^{-11} T/μm and therefore negligible. All measurements were performed at a base temperature of 60 mK. The measurement scheme is shown schematically in Fig. 1(b). The QPC current I_{QPC} for detecting the charge state was measured by initially setting the QPC conductance at half the value of the quantized conductance ($\sim e^2/h$), where its derivative is large enough to detect the charge change in the DQD [16,19]. The transconductance, $dI_{\mathrm{QPC}}/dV_{\mathrm{G2}}$, was measured at the dc QPC bias $V_Q = 0.4$ mV by using a lock-in technique with the frequency set at 13 Hz and with an excitation amplitude of about 1 mV.

Figure 2(a) shows the $dI_{\mathrm{QPC}}/dV_{\mathrm{G2}}$ values for mapping the DQD charge states in the plane of the gate voltages V_{G1} and V_{G3}. The bias voltage for the DQD was set at $V_D = -0.31$ mV. Here, a nonzero bias is needed to lower the Fermi energy of the right lead E_{F2} sufficiently from the ground state in QD2 to avoid thermal fluctuations [see Fig. 1(a)]. The voltage V_{G4} was adjusted to keep the QPC charge sensitivity at its maximum value corresponding to the change in V_{G3}. Figure 2(a) shows a typical honeycomb diagram with the DQD charge states denoted by (N_1, N_2), where N_1 and N_2 correspond to the electron numbers in QD1 and QD2, respectively. Each quasivertical (quasihorizontal) peak line shown in bright (yellow) corresponds to the charge transition between QD1 (QD2) and a nearby lead. The empty state with $(N_1, N_2) = (0, 0)$ can be seen in the lower left of the diagram. The charge state transitions

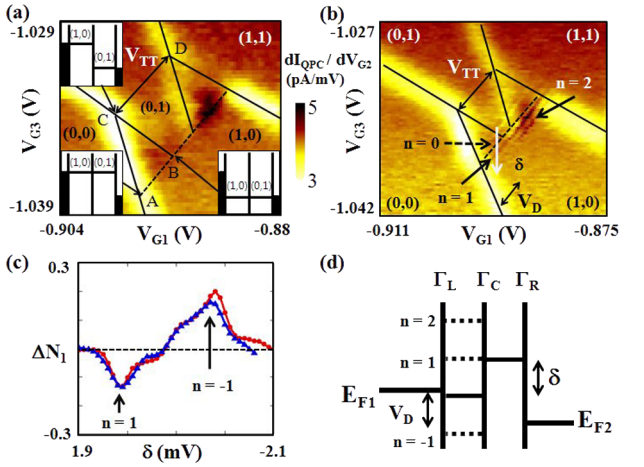

FIG. 2 (color online). Charging diagram between the (1, 0) and (0, 1) states at $V_D = -0.31$ mV (a) without and (b) with MW. The boundary of the transitions between a QD and a nearby lead and that between the two dots is traced by the solid lines and dashed lines, respectively. (N_1, N_2) denotes the DQD charge state where N_1 and N_2 correspond to the electron numbers of QD1 and QD2, respectively. (a) Insets show schematically the charge configurations at a finite bias for three selected points (A, B, C). (b) $n = 0$, $n = 1$, and $n = 2$ denote the zeroth, first, and second excited states due to photon absorption measured for a MW power of -39 dBm and $f_{\mathrm{MW}} = 17.05$ GHz at $B_0 = 2.1$ T. V_{TT} denotes the energy spacing between C and D in (a). (c) Change in the electron number ΔN_1 between (1, 0) and (0, 1) charge states as a function of the energy separation δ. The first PAT peaks obtained by applying MW appear at $B_0 =$ 0.3 T (red dots) and 5 T (blue triangles) with a power of -34 dBm (corresponding to $V_{\mathrm{ac}} = 116$ μeV) and $f_{\mathrm{MW}} =$ 17.05 GHz. (d) Schematic energy diagram of the two ground states of the two dots with the PAT sidebands at a finite V_D.

caused by electron tunneling between either QD1 or QD2 and an adjacent lead and between the two dots are traced by the solid line and the dotted line respectively. We estimated the tunneling rates Γ_L, Γ_R, and Γ_C through the left, right, and center tunneling barriers to be of the order of 100, 0.1, and 1 MHz, respectively, by applying an ac voltage to the MW gate G0. Here, we used the feature that the corresponding transition line becomes narrower as the frequency of the ac signal increases and exceeds the value of $\Gamma_{L(R,C)}$ such that the perturbation on the tunneling barrier due to the ac signal becomes nonadiabatic.

Hereafter, we focus on the PAT transition between the (1, 0) and (0, 1) states for the spin readout experiment. This transition occurs at the boundary between the (1, 0) and (0, 1) charging states, which is defined by two triple points, C and D, for (0, 0)-(0, 1)-(1, 0) and (1, 1)-(0, 1)-(1, 0) [Fig. 2(a)], respectively. For a finite bias V_D, the triple points are expanded to form the triangular regions with a baseline along the (1, 0)-(0, 1) boundary [20,21]. The spacing V_{TT} between the triple points is a measure for $V_{\mathrm{int}} + 2\hbar\Gamma_C$, where $\hbar$ ($= h/2\pi$) is the reduced Planck constant

and $V_{\rm int}$ is the interdot Coulomb energy. Here, $V_{\rm int} + 2\hbar\Gamma_C \approx V_{\rm int}$ because the interdot tunneling coupling $\hbar\Gamma_C \sim 10$ neV was set to be much smaller than $V_{\rm int}$. The baseline length is given by $-eV_D$, and the two triangular regions are spaced by $-eV_D + V_{\rm int}$, where $-e$ is the electron charge. Therefore, we can convert V_{TT} to $V_{\rm int}$ on an energy scale, where $V_{\rm int} = 0.4$ meV. Note that the $(0, 1)$ and $(1, 0)$ states are only degenerate along the diagonal baseline of the two triangles. The insets in Fig. 2(a) show the alignments of the chemical potentials with the DQD charge states at selected points (A, B, C) in the charging diagram to explain the charge state configurations. Figure 2(b) shows the transconductance in the vicinity of the $(1, 0)$-$(0, 1)$ boundary measured for $V_D = -0.31$ mV with MW. When MWs with frequency $f_{\rm MW}$ are employed, photon sidebands to the lowest state in each dot are formed at energies separated by $nhf_{\rm MW}$, where $n = 0, \pm1, \pm2, \ldots$. The positive (negative) integer stands for photon absorption (emission). PAT occurs between the $(1, 0)$ and $(0, 1)$ states when the two states are separated by $\delta = nhf_{\rm MW}$, as shown schematically in Fig. 2(d). The dark lines in Fig. 2(b) indicate PAT with $n = -1$, 0, 1, and 2 measured for $f_{\rm MW} = 17.05$ GHz. The $(1, 0)$-$(0, 1)$ transition with n photons occurs with a probability given by $\Gamma_C J_n(\alpha)^2$, where $J_n(\alpha) = \sum_{k=0}^{\infty} \frac{(-1)^k(\alpha/2)^{n+2k}}{k!\Gamma(n+k+1)}$ is the nth Bessel function for $\alpha = eV_{\rm ac}/hf_{\rm MW}$ and $V_{\rm ac}$ is the MW amplitude. Then the electron charge becomes delocalized between the two dots, which means that the PAT transitions can be detected as a charge change. An estimation, e.g., from the initial state $(1, 0)$ to the delocalized state $[1 - J_n(\alpha)^2/2, J_n(\alpha)^2/2]$, yields (0.83, 0.17) for $n = \pm1$. This change in the charge can now be detected by the QPC. In Fig. 2(c) the change in the electron number ΔN_1 between the $(1, 0)$ and $(0, 1)$ charge states is presented as a function of the energy separation δ. The dots (red) and triangles (blue) represent detailed data measured at $B_0 = 0.3$ and 5 T, respectively. Here, the gate voltage $V_{\rm G3}$ is swept to meet the PAT condition with $\delta = \pm hf_{\rm MW}$. The change in the QPC conductance is converted to that in the electron number ΔN_1 between the $(1, 0)$ and $(0, 1)$ charge states. The peak or dip of ΔN_1 with $n = \pm1$ for both fields is about 0.17 ± 0.04, which agrees with the above estimation. In addition, we estimate an electron temperature $T_e \approx 360 \pm 40$ (520 ± 80) mK without (with) MW using the formula $N_1 \approx 0.5\{1 + \tanh[\delta/(2k_BT_e)]\}$ for $\hbar\Gamma_C \ll k_BT_e$ [19], where k_B is Boltzmann's constant. We find that the PAT forms a hump at $n = 1$, $n = -1$ [Fig. 2(c)] and becomes wider and distorted with increasing MW power. This can be explained by the fact that the PAT between the two dots overlaps the PAT between QD1 and the adjacent lead.

By monitoring the first PAT transition of the $(1, 0)$ state into the $(0, 1)$ state, we are able to readout the spin state for a single electron in the DQD at a relevant external magnetic field B_0. The lowest state of QD1 is lower than that of QD2 by an energy separation $\delta_0 = hf_{\rm MW}$ at $B_0 = 0$ T. The Fermi energy E_{F1} of the lead adjacent to QD1 is located between the two Zeeman states of QD1, where the lower Zeeman state is the up-spin state (ground state) and the higher state is the down-spin state (excited state). The Fermi energy E_{F2} of the other lead is lower than the lowest QD2 state, thus $-eV_D = E_{F1} - E_{F2}$ [see Fig. 1(a)]. We use the temperature as a parameter to initialize the spin configuration of the $(1, 0)$ state in two different ways: only up spin at low temperature and either up spin or down spin at higher temperature. For E_{Z1} [Fig. 1(a)] $> k_BT_e$, an electron only occupies the up-spin state (ground state) in QD1. Therefore, the PAT peak is only present for the up-spin state in the transconductance when $hf_{\rm MW} = hf_{\rm up} = \delta_0 + (1/2)\Delta E_Z$ $(= E_{Z1} - E_{Z2})$, where ΔE_Z is the difference in Zeeman energy between QD1 and QD2. $\Delta E_Z > 0$ indicates the different contributions from the stray field of the micromagnet for the two dots. On the other hand, for $E_{Z1} < k_BT_e$, an electron also occupies the down-spin state in QD1 due to the thermal broadening of E_{F1}. Therefore, another PAT peak corresponding to the down-spin state should appear in the $I_{\rm QPC}$ transconductance at a MW frequency separated by $\Delta f = \Delta E_Z/h$ from the up-spin state in QD1. Actually, we estimate $\Delta f \sim 100 \pm 10$ MHz from the PAT readout experiment [see Fig. 3].

Figure 3 shows the PAT spin readout results as a function of $f_{\rm MW}$ at around 17 GHz, measured for three different external magnetic fields at $B_0 = 5$, 1.1, and 0.6 T. At $B_0 = 5$ T such that $E_{Z1} > k_BT_e$, we observe a single PAT peak

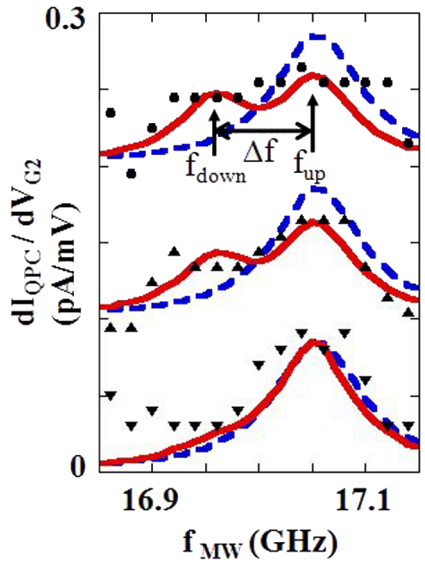

FIG. 3 (color online). PAT spin readout as a function of $f_{\rm MW}$ at around 17 GHz, measured for various external magnetic fields. PAT traces in solid (red) lines and dashed (blue) lines denote theoretical fittings using a master equation for a DQD at 500 and 10 mK, respectively, where $f_{\rm up(down)}$ stands for the PAT frequency of the up (down) spin for B_0 from 0.6 (●), 1.1 (▲), and 5 T (▼). Here, each curve is shifted from the others for clarity.

due to the up-spin interdot transition. As the field decreases to $B_0 = 1.1$ T, another PAT peak due to the down-spin interdot transition starts to appear at a lower f_{MW}. Finally, at $B_0 = 0.6$ T such that $E_{Z1} < k_B T_e$, the two PAT peaks strongly overlap. We fitted the measured data in Fig. 3 using a master equation for the Hamiltonian H for a DQD:

$$\begin{aligned} H &= H_{\mathrm{lead}} + H_D^0 + H_D(t) + H_{\mathrm{tunnel}}, \\ H_{\mathrm{lead}} &= \sum_{a,k} \epsilon_{a,k} C_{a,k}^\dagger C_{a,k}, \\ H_D^0 &= \epsilon_l d_l^\dagger d_l + \epsilon_r d_r^\dagger d_r - \hbar\Gamma_C (d_l^\dagger d_r + d_r^\dagger d_l) + H_C, \\ H_D(t) &= eV_{\mathrm{ac}} \cos(2\pi f_{\mathrm{MW}} t)(d_l^\dagger d_l - d_r^\dagger d_r), \\ H_{\mathrm{tunnel}} &= \sum_k \{t_{L,k} C_{L,k}^\dagger d_l + t_{R,k} C_{R,k}^\dagger d_r + \mathrm{H.c.}\}, \end{aligned} \tag{1}$$

where $C_{a,k}^\dagger (C_{a,k})$ and $d_{l(r)}^\dagger (d_{l(r)})$ are creation (annihilation) operators in the left and right leads $a = L$ and R, respectively, with the momentum k. The $\epsilon_{a,k}$ and $t_{a,k}$ are the energies in the leads and the tunneling coupling, respectively. $\epsilon_{l(r)}$ is the level energy in QD1 (2). H_C represents the Coulomb interaction in a DQD, and is assumed to be infinitely large. H.c. stands for the Hermitian conjugate in H_{tunnel}. Each PAT trace shown with a solid (red) line and a dashed (blue) line exhibits a fitting curve calculated by using the master equation at $T_e = 500$ and 10 mK, respectively. Here, the parameters $\Gamma_L = 120 \pm 80$ MHz, $\Gamma_R = 0.5 \pm 0.4$ MHz, $\Gamma_C = 5 \pm 0.5$ MHz, and $T_e = 500 \pm 50$ mK are chosen to obtain the best fitting. These parameters are in good agreement with those estimated above. The initialization of the spin configuration in the $(1, 0)$ state is determined exactly by the energy configuration between QD1 and the left lead. As seen in Fig. 3 for $B_0 = 5$ T, the up spin is only occupied in QD1 for any temperature smaller than $T_e = 500$ mK. On the other hand, at $T_e = 500$ mK the down-spin state is also occupied in QD1 for a smaller B_0 corresponding to $E_{Z1} \leq k_B T_e$. Finally, the occupation of the two spin states becomes equivalent at about $B_0 = 0.6$ T. Almost the same result as shown in Fig. 3 is obtained for different f_{MW} or δ values. Notice that Γ_C is a key parameter for the observed PAT peak broadening in the fitting. The full width at half maximum of the PAT peak is proportional to Γ_C and almost independent of Γ_L and Γ_R by an order of magnitude. In the present experiment we only performed continuous PAT readouts of the two spin orientations, but it may be important to point out that, in principle, the time needed for the QPC charge detection of the PAT peaks can be less than a few milliseconds, i.e., the electron spin relaxation time [7]. This means that our PAT technique can be applied to the nondestructive readout of both spins. In addition, we point out that by using Co or NiFe instead of Ni for the micromagnet, the two PAT peaks in Fig. 3 should be even more separated by a factor of 3. The spin readout quality would then be significantly improved.

In conclusion, we investigated experimentally PAT spin readout in a DQD including a micromagnet. We observed two PAT peaks corresponding to different spin states. The PAT spacing is consistent with the stray field difference of the magnet. Furthermore, the different spin states are addressable as a function of external magnetic fields.

This work was supported financially by Grants-in-Aid for Scientific Research S (No. 19104007), B (No. 18340081), and Special Coordination Funds for Promoting Science and Technology. S. T. acknowledges support from the QuEST program (BAA-0824). S. T. and Y. T. acknowledge support from MEXT Grant-in-Aid for Scientific Research on Innovative Areas, Contract No. 21102003.

*shin@meso.t.u-tokyo.ac.jp

[1] D. Loss and D. P. DiVicenzo, Phys. Rev. A **57**, 120 (1998).
[2] F. H. L. Koppens *et al.*, Nature (London) **442**, 766 (2006).
[3] K. C. Nowack *et al.*, Science **318**, 1430 (2007).
[4] L. Meier *et al.*, Nature Phys. **3**, 650 (2007).
[5] M. Pioro-Ladrière *et al.*, Nature Phys. **4**, 776 (2008).
[6] E. A. Laird *et al.*, Phys. Rev. Lett. **99**, 246601 (2007).
[7] J. M. Elzerman *et al.*, Nature (London) **430**, 431 (2004).
[8] R. Hanson *et al.*, Phys. Rev. Lett. **94**, 196802 (2005).
[9] T. Meunier *et al.*, Phys. Rev. B **74**, 195303 (2006).
[10] J. Berezovsky *et al.*, Science **314**, 1916 (2006).
[11] H.-A. Engel *et al.*, Phys. Rev. Lett. **93**, 106804 (2004).
[12] S. D. Barrett and T. M. Stace, Phys. Rev. Lett. **96**, 017405 (2006).
[13] J.-P. Zhang *et al.*, J. Phys. Condens. Matter **20**, 395206 (2008).
[14] T. Kodera *et al.*, Physica (Amsterdam) **22E**, 518 (2004).
[15] S. M. Huang *et al.*, arXiv:0904.1046v1.
[16] C. Buizert *et al.*, Phys. Rev. Lett. **101**, 226603 (2008).
[17] Y. Tokura *et al.*, Phys. Rev. Lett. **96**, 047202 (2006).
[18] M. Pioro-Ladrière *et al.*, Appl. Phys. Lett. **90**, 024105 (2007).
[19] J. R. Petta *et al.*, Phys. Rev. Lett. **93**, 186802 (2004).
[20] W. G. van der Wiel *et al.*, Rev. Mod. Phys. **75**, 1 (2002).
[21] R. Hanson *et al.*, Rev. Mod. Phys. **79**, 1217 (2007).